ADVANCED THEORY AND SIMULATIONS
www.advtheorysimul.com

Analytical Physical Model for Organic Metal-Electrolyte-Semiconductor Capacitors

*Larissa Huetter, Adrica Kyndiah, and Gabriel Gomila**

This work presents the analytical physical modeling of undoped organic metal-electrolyte-semiconductor (OMES) capacitors in the framework of the Nernst–Planck–Poisson theory, including the presence of compact interfacial layers. This work derives an exact analytical solution, up to a quadrature, for the stationary electric potential and charge density distributions in both the semiconductor film and the electrolyte solution, and from them the sheet semiconductor charge and the stationary differential capacitance are obtained as a function of the applied voltage. The dependence of these magnitudes on the physical device parameters, like the ionic concentration of the electrolyte, the capacitance of the interfacial compact layers and the injected hole density is then analyzed. This work shows that ionic diffusive effects in the electrolyte can play an important role in the device response, inducing a broadening of the transition from the weak to the strong accumulation regimes. This fact can make that the strong accumulation regime is not achieved in OMES within the usual voltage operation range of these devices. The analytical solution is validated by means of finite element numerical calculations. The implications of the results obtained on the physics of electrolyte gated organic field effect transistors (EGOFETs) are discussed.

1. Introduction

Organic metal-electrolyte-semiconductor (OMES) capacitors are a type of organic metal-insulator-semiconductor (OMIS) capacitor[1] in which the solid dielectric is replaced by an electrolyte. OMES are basic test structures and constitute the basis to understand the physics of more advanced devices, like electrolyte gated organic field effect transistors (EGOFETs).[2] The gate electrode in OMES is in contact with, or immersed in, an electrolyte, which is also in contact with the semiconductor film (**Figure 1**a). In the simplest case, the semiconductor is undoped and impermeable to the penetration of ions. Upon the application of a potential to the gate electrode with respect to the source electrode V_{GS}, electrical double layers (EDLs) form at the gate/electrolyte and semiconductor/electrolyte interfaces, leading to the injection, and accumulation, of holes in the semiconductor, whose concentration is modulated by the applied voltage. The capacitance of an OMES capacitor is, then, dependent on the applied voltage, as in any OMIS capacitor.[1] Three characteristic voltage regimes are expected to exist depending on the level of accumulated free carriers inside the semiconductor (assumed to be holes, namely, weak ($V_{GS} > V_{FB}$), moderate ($V_{GS} < V_{FB}$) and strong ($V_{GS} << V_{FB}$) accumulation regimes, where V_{FB} is the so-called flat band potential[1] (Figure 1b).

The properties of the EDLs, and hence the capacitance of OMES capacitors, depend on the physicochemical properties of the metal/electrolyte and semiconductor/electrolyte interfaces. These interfaces present a rich phenomenology involving ion, water and contaminants adsorption, electrochemical redox reactions, formation of ionic diffusive space charge layers, etc., whose accurate description is rather complex.[3] Usually, to describe them, one resorts to the classical continuum theories. The simplest continuum theory for the EDL was proposed by Helmholtz,[4] and it considers the EDL as a capacitor with specific capacitance c_H, (Helmholtz capacitance). In addition, it also neglects any potential drop in the remaining electrolyte. The whole electrolyte, then, can be substituted by two Helmholtz capacitances, corresponding to the gate/electrolyte $c_{H,G}$, and semiconductor/electrolyte $c_{H,sem}$, interfaces, giving an overall equivalent Helmholtz capacitance $c_H = ({c_{H,G}}^{-1} + {c_{H,sem}}^{-1})^{-1}$. The description of OMES capacitors in the Helmholtz approximation is then

L. Huetter, G. Gomila
Nanoscale Bioelectric Characterization Group
Institute for Bioengineering of Catalunya (IBEC), The Barcelona Institute of Science and Technology (BIST)
Baldiri i Reixac 15-21, Barcelona 08028, Spain
E-mail: gabriel.gomila@ub.edu
A. Kyndiah
Center for Nano Science and Technology
Instituto Italiano di Tecnologia
Via Pascoli, 70/3, Milano 20133, Italy
G. Gomila
Department of Electronics and Biomedical Engineering
Universitat de Barcelona
Martí i Franqués, 1, Barcelona 08028, Spain

The ORCID identification number(s) for the author(s) of this article can be found under https://doi.org/10.1002/adts.202200698

DOI: 10.1002/adts.202200698

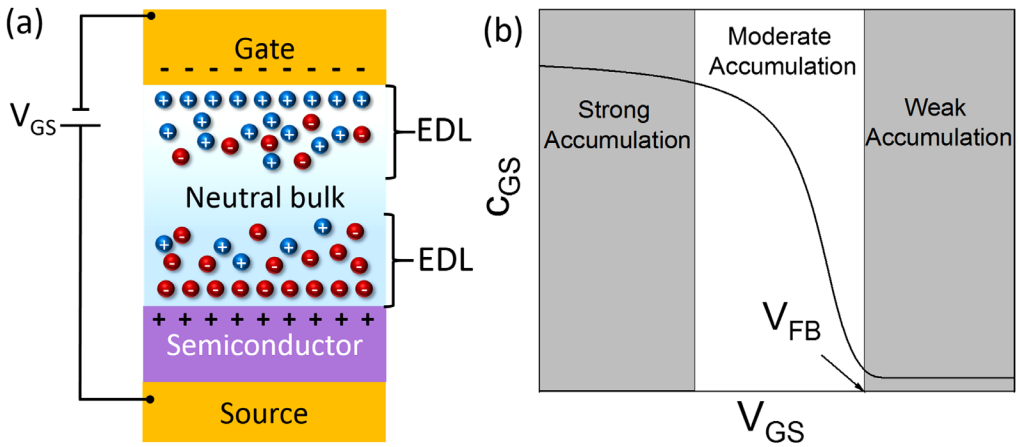

Figure 1. a) Schematic representation of an organic metal/electrolyte/ semiconductor (OMES) capacitor. The electric double layers (EDLs) include the compact and ionic diffusive layers. b) Characteristic voltage regimes of the capacitance of an OMIS capacitor, with the different levels of accumulated carriers in the semiconductor.

equivalent to the description of conventional organic OMIS capacitors, with c_H playing the role of the gate insulator capacitance c_i. A full analytical analysis of undoped OMIS capacitors can be found, for instance, in ref. [1]. The capacitance of EDLs, however, depends on the applied voltage and on the ionic concentration in the electrolyte, effects that are not explicitly included in the Helmholtz approximation. To include them, Gouy[5] and Chapman[6] developed a Poisson–Boltzmann description of the solid/electrolyte interface in which ions accumulate at the interface forming ionic diffusive space charge layers. The Gouy–Chapman theory, however, predicts an unrealistic unbounded exponential increase of the diffusive capacitance with the applied gate voltage.[7] To overcome this unphysical result the Gouy–Chapman theory was further modified by Stern[7] to include an ultrathin compact layer at the solid/electrolyte interface (referred to as the Stern layer). In the Stern–Gouy–Chapman framework the EDL capacitance is dominated by the ionic diffusive capacitance for low applied voltages and by the Stern layer capacitance for larger voltages, offering a more realistic description of solid/electrolyte interfaces. The analytical modeling of OMES in this more realistic framework has not been addressed, yet.

The objective of the present work is precisely to model analytically OMES capacitors within the Stern–Gouy–Chapman framework. To this end, we consider the Nernst–Planck–Poisson (NPP) transport theory of electrolytes, including the presence of interfacial compact layers, which, at equilibrium, is equivalent to the Stern–Gouy–Chapman theory. The NPP theory is more general than the Stern–Gouy–Chapman theory as it allows considering non-equilibrium and time dependent phenomena (e.g., transients or ac frequency response), although we will not discuss them in the present work. An analytical solution (up to a quadrature) for the stationary electric potential and charge density distributions in an undoped OMES capacitor will be derived, from where the differential capacitance and the sheet accumulated semiconductor charge will be determined as a function of the source-gate voltage. The effects of the physical device parameters, like the ionic concentration, the capacitance of the compact layers or the injected hole density, will be then evaluated and analyzed. The relevance of the ionic diffusive effects will be assessed by comparing the predictions of the NPP theory with those of the conventional OMIS capacitor theory[1] (which is equivalent to that for OMES capacitors in the Helmholtz approximation), in which ionic diffusive effects are neglected. Finally, the implications of the results in the understanding of the physics of EGOFETs will be discussed. The analytical solution derived has been verified by means of finite-element numerical calculations. The results presented in the present work can also be applied to OMES capacitors presenting interfacial layers others than the Stern layers, such as functionalization biorecognition layers in biosensors,[8] or phase separated semiconductor layers, sometimes present in some organic semiconductor materials.[9]

2. Nernst–Planck–Poisson Analytical Theory for Undoped OMES Capacitors

Figure 2 shows a schematic representation of the 1D OMES capacitor model considered in the present work.

The semiconductor is assumed to be undoped and impermeable to the penetration of ions and with only one type of carriers (holes), since the source is assumed to inject only one type of carriers, as it is usual in organic semiconductor devices. The electrolyte is characterized by its thickness h_{elec}, dielectric constant ϵ_{elec}, ionic concentration n_0, and ionic mobilities μ_{ion}. The semiconductor film, on its side, is characterized by its thickness h_{sem}, dielectric constant ϵ_{sem}, and hole mobility μ_p, assumed isotropic for simplicity. For the stationary (low frequency) conditions considered here, in which no net dc current flows, the mobilities do not play any role. At the gate/electrolyte and semiconductor/electrolyte interfaces compact ultrathin dielectric layers characterized by their respective specific capacitances, c_G and c_{int} are assumed to exist. A fixed charge at the surface of the gate interfacial layer with surface density $q_{fix,G}$, is also considered. Finally, the source-semiconductor interface is assumed to be ideal, what implies that the hole carrier density at the source electrode is fixed to a given value p_S (see below).

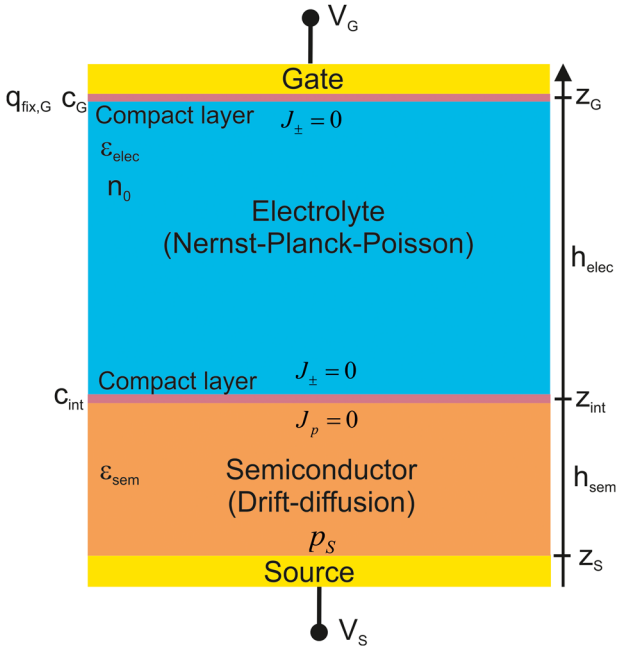

Figure 2. Schematic representation of the 1D OMES capacitor model considered in the present work with the physical parameters and theoretical frameworks considered.

The electric potential $\varphi_{sem}(z)$, and hole density $p(z)$, distributions in the semiconductor are described by means of the 1D drift–diffusion model for an undoped semiconductor.

$$-\varepsilon_0\varepsilon_{sem}\frac{\partial^2\varphi_{sem}}{\partial z^2} = ep \tag{1}$$

$$\frac{\partial p}{\partial t} + \frac{\partial J_p}{\partial z} = 0 \tag{2}$$

$$J_p = -\mu_p p\frac{\partial\varphi_{sem}}{\partial z} - D_p\frac{\partial p}{\partial z} \tag{3}$$

here, e is the electron charge, J_p the hole number flux density, and D_p the hole diffusion coefficient, which is assumed to be related to the hole mobility μ_p by Einstein's relation for non-degenerate semiconductors $D_p = \mu_p k_B T/e$, where k_B is Boltzmann's constant and T the temperature. Equations (1)–(3) are valid in the range $z_S \le z \le z_{\text{int}}^-$ (Figure 2), where $z_{\text{int}}^- = z_{\text{int}} - \delta_{\text{int}}/2$, with δ_{int} being the thickness of the semiconductor/electrolyte compact interfacial layer. The electric potential $\varphi_{elec}(z)$, and ionic density distributions in the electrolyte $n_\pm(z)$ (assumed to be 1:1) are described by means of the 1D NPP model, which is formally identical to the drift–diffusion model for semiconductors, although the underlying transport physics is, of course, different.

$$-\varepsilon_0\varepsilon_{elec}\frac{\partial^2\varphi_{elec}}{\partial z^2} = e\left(n_+ - n_-\right) \tag{4}$$

$$\frac{\partial n_\pm}{\partial t} + \frac{\partial J_\pm}{\partial z} = 0 \tag{5}$$

$$J_\pm = -\mu_\pm n_\pm\frac{\partial\varphi_{elec}}{\partial z} - D_\pm\frac{\partial n_\pm}{\partial z} \tag{6}$$

here, $J_\pm$ are the ionic number flux densities, $\mu_\pm$ the ionic mobilities and $D_\pm$ the ionic diffusion coefficients, related through Einstein's relation for diluted ionic solutions $D_\pm = \mu_\pm k_B T/e$. We assumed the electrolyte to be 1:1 symmetric, so that $\mu_+ = \mu_- = \mu_{ion}$. Equations (4)–(6) are valid for $z_{\text{int}}^+ \le z \le z_G^-$ where $z_{\text{int}}^+ = z_{\text{int}} + \delta_{\text{int}}/2$ and $z_G^- = z_G - \delta_G/2$with δ_G being the thickness of the gate compact interfacial layer. (Figure 2). The initial concentrations of the two ionic species are assumed to be the same and equal to n_0.

At the source electrode we assumed a fixed hole density boundary condition corresponding to an ideal injecting diffusive contact,[10] namely

$$p\left(z_S{}^+\right) = p_S \tag{7}$$

F or simplicity, we neglected non-ideal hole injection effects related to interfacial polarization and disorder[11] or to the presence of interfacial states.[12] Within these approximations, p_S can be taken as a constant independent from the applied source-gate voltage and dependent only on the injection barrier height and density of states (see Appendix A). Zero flux boundary conditions are assumed at the gate/electrolyte and semiconductor/electrolyte interfaces.

$$J_p\left(z_{\text{int}}^-\right) = 0, J_\pm\left(z_{\text{int}}^+\right) = 0, J_\pm\left(z_G^-\right) = 0 \tag{8}$$

Accordingly, no exchange of charges (ions or holes) occurs at the semiconductor/electrolyte and gate/electrolyte interfaces, implying the lack of faradaic reactions and of gate leakage currents. These conditions imply that the total number of ions in the electrolyte remains constant and equal to the initial one. Finally, the interfacial layers are described by means of distributed capacitance boundary and continuity conditions. At the gate electrode one has

$$\varepsilon_0\varepsilon_{elec}\frac{\partial\varphi_{elec}\left(z_G^-\right)}{\partial z} = -c_G\left[\varphi_{elec}\left(z_G^-\right) - V_G + \Delta V_{qG}\right] \tag{9}$$

where V_G is the potential of the gate electrode and

$$\Delta V_{qfix} = q_{fix,G}/c_G \tag{10}$$

the voltage-shift due to the fixed charge at the gate compact interfacial dielectric layer. For the semiconductor/electrolyte interface one similarly has

$$\varepsilon_0\varepsilon_{elec}\frac{\partial\varphi_{elec}\left(z_{\text{int}}^+\right)}{\partial z} = c_{\text{int}}\left[\varphi_{elec}\left(z_{\text{int}}^+\right) - \varphi_{sem}\left(z_{\text{int}}^-\right)\right] \tag{11}$$

$$\varepsilon_{sem}\frac{\partial\varphi_{sem}\left(z_{\text{int}}^-\right)}{\partial z} = \varepsilon_{elec}\frac{\partial\varphi_{elec}\left(z_{\text{int}}^+\right)}{\partial z} \tag{12}$$

Finally, at the bottom of the semiconductor film, in contact with the source electrode, we assume a fixed potential boundary condition.

$$\varphi_{sem}\left(z_S^+\right) = V_S \tag{13}$$

which is valid since the source/semiconductor interface is assumed to be ideal and non-polarizable. We also assume, for simplicity, that there is no difference in the metal work functions

of the source and gate electrodes. Under such conditions, the source-gate voltage is simply given by $V_{GS} = V_G - V_S$. If a work function difference existed, it should be subtracted from the value of V_{GS}.

Equations (1)–(6), subject to the boundary and continuity conditions in Equations (7–9) and (11–13) constitute a complete set of equations to determine the electric potential and free carrier concentrations in an undoped OMES capacitor in the NPP framework including the presence of compact interfacial dielectric layers. We note that in this model the Stern layer of the Stern–Gouy–Chapman model is represented by the series combination of c_{int} and c_G and the Gouy–Chapman theory by the resolution of the Poisson equation. This model can be solved analytically (up to a quadrature) under stationary conditions. The details of the derivation are presented in Appendix A. The electric potential distribution in the semiconductor and in the electrolyte, $\varphi_{sem}(z)$ and $\varphi_{elec}(z)$, respectively, are given by (the sign convention is explained in Appendix B)

$$\frac{e\left[\varphi_{sem}(z)-V_S\right]}{k_BT} = -\ln\left\{\beta\tan^2\left[\mp\frac{(z-z_S)}{2L_{Ds}}\sqrt{\beta} + \tan^{-1}\left(\sqrt{\frac{1}{\beta}-1}\right)\right]+\beta\right\}, z_S \le z \le z_{\text{int}}^- \tag{14}$$

$$\frac{z-z_G}{L_D} = \mp f \int_{\frac{e\Delta\varphi_{elec}(\beta)}{2k_BT}}^{\frac{e\left[\varphi_{elec}(z)-V_S\right]}{k_BT}+\frac{e\left(V_{GS}-\Delta V_G\right)}{2k_BT}\mp\frac{c_{sem}}{c_G}\sqrt{\beta(\alpha(\beta)-1)}+\frac{e\Delta\varphi_{sol}(\beta)}{2k_BT}} \frac{dy}{\sqrt{2\cosh(y)-b\left(\beta,f\right)}}, \quad z_{\text{int}}^+ \le z \le z_G^- \tag{15}$$

where

$$b\left(\beta,f\right) = 2\cosh\left[\frac{e\Delta\varphi_{elec}(\beta)}{2k_BT}\right] - \left(\frac{c_{sem}}{c_{elec}}\right)^2 f^2\beta\left[\alpha(\beta)-1\right] \tag{16}$$

$$\frac{e\Delta\varphi_{elec}(\beta)}{k_BT} = \frac{e\left(V_{GS}-\Delta V_{qfix}\right)}{k_BT} + \ln\left[\beta\alpha(\beta)\right] \pm \frac{c_{sem}}{c_{\text{int},eq}}\sqrt{\beta\left[\alpha(\beta)-1\right]} \tag{17}$$

$$\alpha(\beta) = 1+\tan^2\left[\mp\frac{h_{sem}}{2L_{Ds}}\sqrt{\beta}+\tan^{-1}\left(\sqrt{\frac{1}{\beta}-1}\right)\right] \tag{18}$$

Here, $\Delta\varphi_{elec} = \varphi_G^- - \varphi_{\text{int}}^+$ is the voltage drop across the electrolyte along the ionic diffusive space charge layers. Moreover, c_{elec} and c_{sem} are the characteristic electrolyte and semiconductor diffusive capacitances, respectively.

$$c_{elec} = \frac{\varepsilon_0\varepsilon_{elec}}{L_D},\ c_{sem} = \frac{\varepsilon_0\varepsilon_{sem}}{L_{Ds}} \tag{19}$$

with L_D and L_{Ds} being, respectively, the electrolyte and semiconductor Debye screening lengths

$$L_D = \sqrt{\frac{k_BT\varepsilon_0\varepsilon_{elec}}{2e^2n_0}},\ L_{Ds} = \sqrt{\frac{k_BT\varepsilon_0\varepsilon_{sem}}{2e^2p_S}} \tag{20}$$

For symmetry reasons we included also a factor 2 in the definition of L_{Ds}. Furthermore, $c_{int,eq}$ is the equivalent interfacial capacitance

$$c_{\text{int},eq} = \left(\frac{1}{c_{\text{int}}}+\frac{1}{c_G}\right)^{-1} \tag{21}$$

Finally, β and f are the solutions of the 2×2 non-linear system of equations

$$\frac{h_{elec}}{2L_D} = \mp f\int_0^{\frac{e\Delta\varphi_{elec}(\beta)}{2k_BT}} \frac{dy}{\sqrt{2\cosh(y)-b\left(\beta,f\right)}} \tag{22}$$

$$\frac{h_{elec}}{2L_D} = \mp\frac{1}{f}\int_0^{\frac{e\Delta\varphi_{elec}(\beta)}{2k_BT}} \frac{\cosh(y)}{\sqrt{2\cosh(y)-b\left(\beta,f\right)}}dy \tag{23}$$

The parameters β and f are functions of the applied voltage V_{GS} through the functions $b(\beta,f_{sol})$ and $\Delta\varphi_{elec}(\beta)$, which depend on it (see Equations (16) and (17)).

The parameter β is related to the derivative of the electric potential at the source electrode (see Appendix A)

$$\beta = 1-\left(\frac{eL_{Ds}}{k_BT}\right)^2\left(\frac{d\varphi_S}{dz}\right)^2 \tag{24}$$

while f is related to the average electrochemical potential of the ions in the electrolyte solution $\bar{\phi}$ (see Appendix A)

$$f = \exp\left(\frac{\tilde{\mu}_{n_0}-\bar{\phi}}{2k_BT}\right) \tag{25}$$

where $\tilde{\mu}_{n_0}$ is the chemical potential of the ions at the concentration n_0. By definition for $|d\varphi_S/dz| < k_BT/eL_{Ds}$ one has $0<\beta<1$, while for $|d\varphi_S/dz| > k_BT/eL_{Ds}$ one has $\beta<0$. When $\beta<0$, Equations (14) and (15) are still valid, but they should be evaluated in the complex plane, leading to real values for the potentials. Alternatively, one can use explicit real expressions (see Appendix C). On the other side, f takes values very close to 1 (since $\bar{\phi}\approx\tilde{\mu}_{n_0}$, in general), except when the ionic diffusive space charge layers overlap, which is not usually the case in realistic OMES capacitor geometries.

The volumetric charge densities in the semiconductor film, $\rho_{sem}(z) = ep(z)$, and electrolyte, $\rho_{elec}(z) = e(n_+(z) - n_-(z))$, are given, respectively, by (see Appendix A)

$$\rho_{sem}(z) = \frac{ep_S\beta}{\cos^2\left[\mp\frac{(z-z_S)}{2L_{Ds}}\sqrt{\beta}+\tan^{-1}\left(\sqrt{\frac{1}{\beta}-1}\right)\right]} \tag{26}$$

$$\rho_{elec}(z) = -\frac{2en_0}{f^2}\sinh\left[\frac{e\left(\varphi_{elec}(z)-V_G\right)}{k_BT}\mp\frac{c_{sem}}{c_G}\sqrt{\beta\left(\alpha(\beta)-1\right)}+\frac{e\Delta\varphi_{elec}(\beta)}{2k_BT}\right] \tag{27}$$

The surface charge densities accumulated at the gate and source electrodes, q_G and q_S, respectively, are calculated from the derivatives of the electric potential at the source and gate interfaces, giving (see Appendix A)

$$q_S = \mp sign(\beta) c_{sem} \frac{k_B T}{e} \sqrt{1-\beta} \tag{28}$$

$$q_G = \mp c_{sem} \frac{k_B T}{e} \sqrt{\beta\left(\alpha\left(\beta\right)-1\right)} + q_{fix,G} \tag{29}$$

rather than by solving Equations (22) and (23). The values of β_H for an OMIS capacitor differ only slightly from those of β for an OMES capacitor, but this difference is relevant since it contains the ionic diffusive effects in the electrolyte (see below). We verified that the solution for an OMIS capacitor obtained proceeding as indicated above is fully equivalent to the one derived in ref. [1] as should be. In here, we derived, in addition, an explicit analytical expression for the differential capacitance of an OMIS capacitor by using Equation (32) in Equation (31).

$$c_{GS} = c_{\mathrm{int},eq} \left\{ 1 \pm 2 \frac{c_{\mathrm{int},eq}}{c_{sem}} \frac{\left[\sqrt{1-\beta_H} + (\pm)(\mp)\sqrt{\beta_H\left(\alpha\left(\beta_H\right)-1\right)}\left[\mp\frac{h_{sem}}{2L_{Ds}}\sqrt{1-\beta_H} - sign\left(\beta_H\right)\right]\right]}{\left[\sqrt{1-\beta_H}\sqrt{\beta_H\left(\alpha\left(\beta_H\right)-1\right)} + (\pm)(\mp)\beta_H\alpha\left(\beta_H\right)\left[\mp\frac{h_{sem}}{2L_{Ds}}\sqrt{1-\beta_H} - sign\left(\beta_H\right)\right]\right]} \right\}^{-1} \tag{33}$$

The sheet charge accumulated in the semiconductor film q_{sem} can be calculated either by integration of the semiconductor volumetric charge density in Equation (26) or from the charge conservation relationship $q_{sem} = -q_G - q_{G,int} - q_S$. In both cases one obtains

$$q_{sem} = c_{sem} \frac{k_B T}{e} \left[\pm sign\left(\beta\right)\sqrt{1-\beta} \pm \sqrt{\beta\left(\alpha-1\right)}\right] \tag{30}$$

Finally, the stationary source-gate differential capacitance c_{GS} is obtained from the surface charge accumulated at the gate electrode q_G (Equation (28)) as $c_{GS}(V_{GS}) = \partial q_G(V_{GS})/\partial V_{GS}$, giving

$$c_{GS}\left(V_{GS}\right) = c_{sem} \frac{k_B T}{e} \frac{\partial}{\partial V_{GS}} \sqrt{\beta\left(\alpha-1\right)} \tag{31}$$

No simple analytical relationship could be derived for the differential capacitance, so we evaluated it numerically. This expression completes the analytical resolution of the model.

The solution for an OMIS capacitor,[1] or for an OMES capacitor in the Helmholtz approximation, can be obtained from the solution just derived by simply imposing that the voltage drop in the ionic diffusive space charge layers of the electrolyte is zero, that is, $\Delta\varphi_{elec}(\beta_H) = \varphi_G^+ - \varphi_{\mathrm{int}}^- = 0$. This condition leads to the following implicit expression to determine the parameter β_H

$$V_{GS} = \Delta V_G - \frac{k_B T}{e} \ln\left[\beta_H \alpha\left(\beta_H\right)\right] \mp \frac{k_B T}{e} \frac{c_{sem}}{c_{\mathrm{int},eq}} \sqrt{\beta_H\left[\alpha\left(\beta_H\right)-1\right]} \tag{32}$$

The semiconductor electric potential $\varphi_{sem}(z)$ and charge density $\rho_{sem}(z)$, the accumulated charges in the semiconductor, source and gate electrodes, q_{sem}, $q_{S,}$ and q_G, respectively, and the differential capacitance, c_{GS}, for an OMIS are still given by Equations (14), (26), (28)–(31), respectively, by substituting $c_{int,eq}$ by the insulator capacitance c_i (or by the overall Helmholtz capacitance c_H) and by using the parameter β_H obtained from Equation (32),

This expression should be combined with Equation (32), to obtain a parametric explicit expression.

In the definition of the sign convention (see Appendix B), a characteristic hole density p_S^* was introduced,

$$p_S^* = \frac{\pi^2}{2} \frac{k_B T \epsilon_0 \epsilon_{sem}}{e^2 h_{sem}^2} \tag{34}$$

This hole density, in the absence of any doping density, can be used to define a "flat-band" potential as

$$V_{FB} = \Delta V_{qfix} + \frac{k_B T}{e} \ln\left(\frac{p_S}{p_S^*}\right) \tag{35}$$

This "flat-band" potential does not imply that the bands are indeed flat, since this never happens in an undoped semiconductor, but it rather indicates the voltage at which the capacitance passes from the weak to the moderate accumulation regimes, as will be shown below. This definition is valid for both OMES and OMIS capacitors.

3. Numerical Verification of the Analytical Solution and Results

To verify the analytical solution, we have solved the NPP model for an OMES capacitor numerically by means of the finite element method. To this end we used Comsol Multiphysics 5.5 and the built-in equation-based modeling tool. The existing built-in multiphysics models did not include the compact interfacial capacitances at all electrolyte interfaces. The solution was obtained by using a time dependent solver applied to the time dependent NPP model. A software interface written in Matlab (MathWorks) has been used to automatize the calculations and represent the results. The analytical expressions, on its side, have been evaluated by using Wolfram Mathematica 11.2. This software tool can handle calculations with extremely high accuracy and precision, necessary to deal with the extremely long tails of some

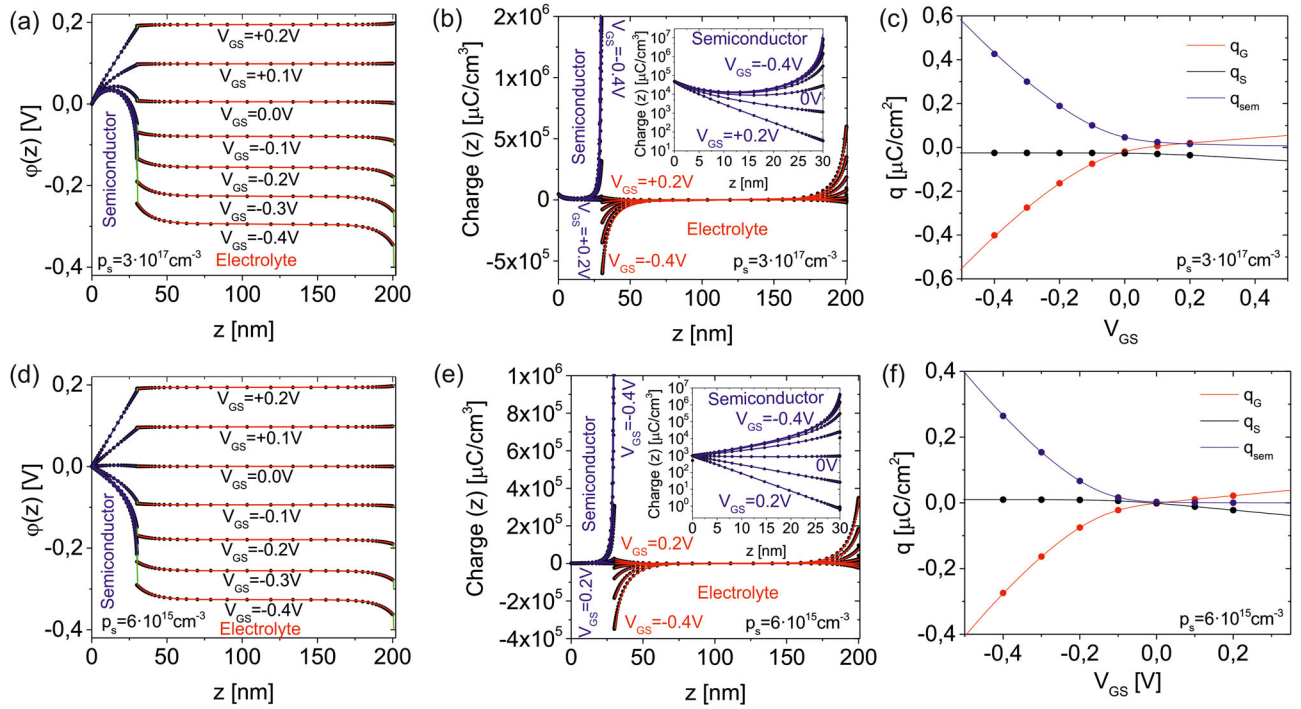

Figure 3. a–c) Electric potential, volumetric charge densities, and accumulated surface (or sheet) charges in an OMES capacitor for $p_S = 3{\cdot}10^{17}\text{cm}^{-3}$ for different source-gate voltages. The continuous lines correspond to the analytical solution (Equations (14) and (15); Equations (26) and (27); and Equations (28), (29) and (30), respectively) with the parameters β and f obtained by solving Equations (22) and (23) (see Appendix E). The blue, green, and red colors correspond to the semiconductor, interfacial compact layers, and electrolyte regions, respectively. The symbols correspond to the numerical resolution of the model by means of the finite element method. Inset in b): Charge density across the semiconductor in a linear-log representation. d–f) idem to a–c) but for $p_S = 6{\cdot}10^{15}\text{cm}^{-3}$. Parameters of the calculation, if not otherwise stated: $\epsilon_{sem} = 4$, $\epsilon_{elec} = 78$, $n_0 = 1$ mM, $h_{sem} = 30$ nm, $h_{elec} = 170$ nm, $c_G = 7.3$ μF cm^{-2}, $c_{int} = 3.65$ μF cm^{-2}, and $q_{fix,G} = 0$ C m^{-2}. For these parameters: $L_D = 9.6$ nm, $c_{elecl} = 7.2$ μF cm^{-2}, $c_{int,eq} = 2.43$ μF cm^{-2}, $c_{geom} = 0.12$ μF cm^{-2}, and $p_S^* = 3.12{\cdot}10^{16}$ cm^{-3}. Moreover, $L_{Ds} = 3.1$ nm, $c_{sem} = 1.15$ μF cm^{-2}, and $V_{FB} = 0.06$ V for $p_S = 3{\cdot}10^{17}\text{cm}^{-3}$. Finally, $L_{Ds} = 21.8$ nm, $c_{sem} = 0.16$ μF cm^{-2}, and $V_{FB} = -0.04$ V for $p_S = 6{\cdot}10^{15}\text{cm}^{-3}$.

of the analytical expressions. To speed up the calculations, we have expressed Equations (15), (22) and (23) in terms of incomplete elliptic integrals (see Appendix D). In the numerical solution of the system of equations to determine the parameters f and β (Equations (22) and (23)) we used as initial values $f_0 = 1$ and the root of $\Delta\varphi_{elec}(\beta_0) = 0$, which corresponds to the β_H values of the Helmholtz approximation.

The following set of physical parameters, if not otherwise stated, have been considered in the calculations: $\epsilon_{sem} = 4$, $\epsilon_{elec} = 78$, $n_0 = 10$ mM, $p_S = 3{\cdot}10^{17}$ cm^{-3}, $\mu_p = 0.034$ cm^{2}V s^{-1}, $h_{sem} = 30$ nm, $h_{elec} = 100$ μm, $c_G = 7.3$ μF cm^{-2}, $c_{int} = 3.65$ μF cm^{-2}, and $q_{fix,G} = 0$ μC cm^{-2}. For this set of parameters one has $L_D = 3.0$ nm, $L_{Ds} = 3.1$ nm, $c_{sem} = 1.15$ μF cm^{-2}, $c_{elec} = 2.27$ μF cm^{-2}, $c_{int,eq} = 2.43$ μF cm^{-2}, $c_{geom} = \epsilon_0\epsilon_{sem}/h_{sem} = 0.12$ μF cm^{-2}, $p_S^* = 3.12{\cdot}10^{16}$ cm^{-3}, and $V_{FB} = 0.06$ V.

Figure 3a,b (res. 3d and 3e) (continuous lines) show, respectively, the electric potential and charge density distributions across the OMES capacitor for $p_S = 3{\cdot}10^{17}\text{cm}^{-3} > p_S^*$ (respectively, $p_S = 6{\cdot}10^{15}\text{cm}^{-3} < p_S^*$) and for -0.4V < V_{GS} < +0.2 V. The "flat-band" potentials for $p_S = 3{\cdot}10^{17}\text{cm}^{-3}$ and $p_S = 6{\cdot}10^{15}\text{cm}^{-3}$ are, respectively, $V_{FB} = 0.06$ V and $V_{FB} = -0.04$ V. The blue, red, and green lines refer, respectively, to the semiconductor, electrolyte and compact interfacial layers. For a proper visualization of the different space charge layers we took a small value for the thickness of the electrolyte, $h_{sol} = 170$ nm (in the rest of the figures a more realistic value $h_{sem} > 10$ μm has been used). The values of β and f corresponding to Figure 3 are shown in Appendix E. The insets in Figure 3b,e show the charge density across the semiconductor film in linear-log representation. The symbols in Figure 3 represent the results of the finite element numerical calculations. The agreement with the analytical solution is perfect as it corresponds to an exact solution of the problem, thus verifying the analytical expressions derived.

For $V_{GS} = V_{FB}$ ("flat band" conditions) the charge density in the (undoped) semiconductor is of the order of the injected charge ep_S, and almost null in the electrolyte, where practically no diffusive space charge layers are formed. For $V_{GS} > V_{FB}$, the semiconductor gets depleted from holes with respect to when $V_{GS} = V_{FB}$ and the charge density tends to show an exponential decay across the semiconductor film for high enough voltages ($V_{GS} >> V_{FB}$), (see insets in Figure 3b,e). The semiconductor, in this voltage range, behaves like an insulator, with a specific capacitance given by its geometric capacitance $c_{geom} = \epsilon_0\epsilon_{sem}/h_{sem}$ = 0.12 μF cm^2. This capacitance is usually much smaller than the ionic diffusive capacitance of the electrolyte c_{elec}, and hence the applied potential mostly drops in the semiconductor film

and, eventually, at the interfacial compact layers. The potential in the semiconductor, in this voltage range, can be approximated by a linear function (see Figure 3a,c).,

$$\varphi_{sem}(z) \approx V_S + \frac{(z - z_S)}{h_{sem}} \frac{V_{GS}}{1 + \frac{c_{geom}}{c_{\text{int},eq}}}, V_{GS} >> V_{FB} \quad (36)$$

From this dependence (by substituting Equation (36) into Equation (26)) one obtains the exponential dependence of the charge density in the semiconductor displayed in the insets of Figure 3b,e,

$$\rho_{sem}(z) \approx e p_S \exp\left[-\frac{eV_{GS}}{k_B T} \frac{1}{1 + \frac{c_{geom}}{c_{\text{int},eq}}} \frac{(z - z_S)}{h_{sem}} \right], V_{GS} >> V_{FB} \quad (37)$$

For $V_{GS} < V_{FB}$, instead, holes are injected into the semiconductor and accumulate at the semiconductor surface forming the characteristic quasi-2D conducting channel of FET devices in accumulation mode (see Figure 3b,e). Owing to the accumulation of holes, the diffusive capacitance of the semiconductor film increases significantly, and it becomes higher and comparable to those of the electrolyte and compact interfacial layers. The applied source-gate voltage, then, redistributes among the different parts of the capacitor. As a result, ionic diffusive space charge layers develop at the semiconductor/electrolyte and gate/electrolyte interfaces, whose net accumulated charges, and capacitances, increase when the applied source-gate voltage is made more negative. For high enough negative voltages ($V_{GS} << V_{FB}$) the capacitance of the diffusive ionic space charge layers becomes much higher than those of the compact layers and of the semiconductor film, in series with them, at which point any additional applied source-gate voltage will drop almost exclusively at the interfacial compact layers (see Figure 3a,c, green lines). The drop of potential at each compact layer is inversely proportional to the corresponding interfacial capacitance c_G or c_{int}, while the overall potential drop at the compact layers is inversely proportional to the equivalent interfacial capacitance $c_{int,eq}$ In this voltage regime, the density of accumulated holes at the semiconductor surface can become very large (exceeding 10^{19} cm^{-3}, see Figure 3b,e). When this occurs, one should include degeneracy effects in the description, as done, for instance, in ref. [1] for the case of OMIS capacitors. Similarly, if the ionic concentration in the ionic diffusive space charge layers is very high (above 1), one should include non-ideal ionic density effects in the description of the electrolyte.[13,14] For simplicity, we have not included these non-ideal effects in the present work.

The electric potential shows two characteristic behaviors depending on whether the value of the injected hole density p_S is larger or smaller than p_S^* (strictly speaking a third regime exists for $4/\pi^2 p_S^* \le p_S \le p_S^*$ but which is very narrow and we omit it from the discussion). For $p_S > p_S^*$ the potential never gets flat at the source electrode and hence it shows a maximum for all negative voltages (Figure 3a). Instead, for $p_S < p_S^*$ at a given voltage the potential gets flat at the source electrode and the maximum disappears for more negative voltages. These two behaviors can lead to slightly different behaviors of the OMES capacitor, which are not relevant for the present work (see ref. [1] for a discussion of this point for the case of OMIS capacitors).

Figure 3c,f shows the surface charges accumulated at the gate and source electrodes q_S and q_G (black and red continuous lines, respectively), and the sheet charge accumulated in the semiconductor film q_{sem}, (blue continuous line) as a function of the source-gate voltage V_{GS}, for the two hole injected densities p_S considered above, respectively. The charges have been calculated from Equations (28), (29), and (30). As before the symbols correspond to the results of the finite element numerical calculations, which fully agree with the analytical results.

For high enough positive voltages $V_{GS} >> V_{FB}$ the sheet semiconductor charge q_{sem}, can be approximated by the expression resulting of the integration of Equation (37), that is

$$q_{sem} \approx e p_s h_{sem} \left(1 + \frac{c_{geom}}{c_{\text{int},eq}}\right) \frac{k_B T}{e V_{GS}} \left(1 - \exp\left[-\frac{eV_{GS}}{k_B T} \frac{1}{1 + \frac{c_{geom}}{c_{\text{int},eq}}} \right]\right), \quad V_{GS} >> V_{FB} \quad (38)$$

This expression shows an initial exponential decay followed by an inverse decay with the source-gate voltage V_{GS}. The charges accumulated at the source and gate electrodes q_S and q_G tend to increase approximately linearly with the applied voltage showing slopes with equal magnitude but opposite signs. Therefore, for $V_{GS} >> V_{FB}$ the structure behaves like a capacitor in which the (depleted) semiconductor and the compact interfacial layers play the role of the dielectric. Consequently, the capacitance is dominated by the equivalent capacitance resulting from the series combination of the semiconductor geometric capacitance, c_{geom}, and the equivalent capacitance of the compact interfacial layers, $c_{int,eq}$.

For source-gate voltages below the "flat-band" potential $V_{GS} < V_{FB}$, q_{sem} and q_G both increase due to the accumulation of carriers in the semiconductor. For large enough negative voltages the charges tend to show similar magnitude and opposite signs. At the same time, q_S becomes negligible. We observe that q_S changes sign when $p_S < p_S^*$ and it does not do it when $p_S > p_S^*$, although this fact has not an apparent impact in the results. Therefore, for $V_{GS} < V_{FB}$ the structure behaves like a capacitor in which the semiconductor film and the gate electrode play the role of the plates and with the electrolyte playing the role of the dielectric. The overall device capacitance is, then, determined by the capacitance of the electrical double layers at the gate/electrolyte and semiconductor/electrolyte interfaces (including both the compact and the ionic diffusive capacitances). Asymptotically, when the behavior is dominated by the compact interfacial layers, the accumulated charges q_{sem} and q_G tend to an approximately linear dependence with the source-gate voltage (not shown in the graphs),

$$q_{sem} \approx -q_G \approx c_{DL}\left(-V_{GS} + V_{TH}\right), V_{GS} << V_{FB} \quad (39)$$

This dependence is characteristic of field effect devices. However, the voltages at which such behavior is attained in OMES usually lye outside the operational voltage range of these devices (see below).

Figure 4a–c shows the stationary differential capacitance c_{GS} as a function of the source gate voltage V_{GS} for, respectively, different electrolyte ionic concentrations n_0, equivalent interfacial

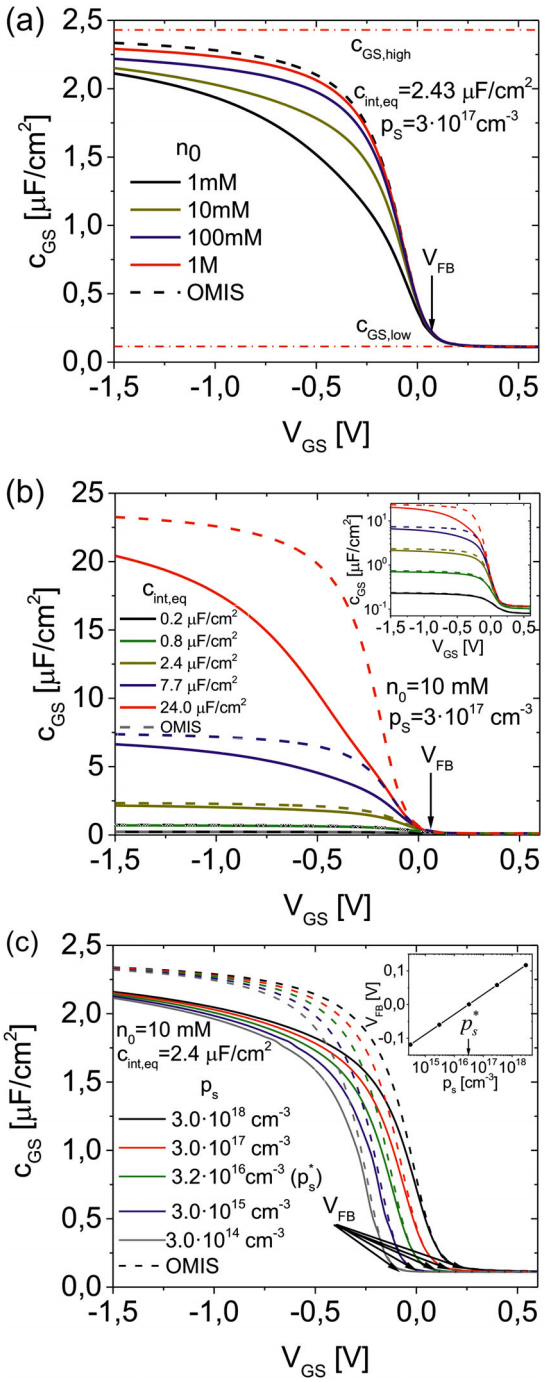

Figure 4. Capacitance of an OMES capacitor c_{GS} as a function of the source-gate voltage V_{GS} for different a) ionic concentrations of the electrolyte n_0, b) interfacial capacitances $c_{int,eq}$ and c) hole injected carrier densities p_S. The dashed lines represent the predictions for an OMIS capacitor with $c_i = c_{int,Equation}$ The red dot-dashed lines in (a) represent the limiting values $c_{GS,low}$ and $c_{GS,high}$ in Equations (40) and (41), respectively. Inset in (b): same data but in log-linear representation. Inset in (c): (symbols) shift of the capacitance curves with respect to the curve for $p_S = p_S^*$. The continuous line corresponds to the predictions of Equation (35). Parameters, unless otherwise stated: $\epsilon_{sem} = 4$, $\epsilon_{elec} = 78$, $n_0 = 10$ mM, $h_{sem} = 30$ nm, $h_{elec} = 100$ μm, $c_G = 7.3$ μF cm^{-2}, $c_{int} = 3.65$ μF cm^{-2} ($c_{int,eq} = 2.43$ μF cm^{-2}), $q_{fix,G} = 0$ C m^{-2}, $p_S = 3{\cdot}10^{17}$cm^{-3}. For these parameters, $c_{geom} = 0.12$ μF cm^{-2}, $V_{FB} = 0.058$ V.

compact capacitances $c_{int,eq}$, and injected hole densities p_S. The inset in Figure 4b shows the data of the main panel but plotted in a linear-log representation.

The differential capacitance has been calculated from Equation (31), with the values of β obtained by solving Equations (22) and (23). For comparison, we have also plotted in Figure 4 (dashed lines) the capacitance corresponding to an OMIS capacitor[1] (or to an OMES capacitor in the Helmholtz approximation), in which ionic diffusive effects in the electrolyte are neglected. The capacitance of the OMIS has been calculated by means of the parametric expression given by Equations (32) and (33). The calculations in Figure 4 have been done for a thick electrolyte ($h_{elec} = 100$ μm). We note that for h_{elec} larger than a few micrometers the results are independent from the actual thickness of the electrolyte. For $V_{GS} > V_{FB}$ (weak accumulation regime) the capacitance c_{GS} tends to a constant value determined by the series combination of the geometric capacitance of the semiconductor c_{geom}, and the equivalent interfacial capacitance $c_{int,eq}$, as advanced above (bottom red dot-dashed line in Figure 4a)

$$c_{GS,low} = \frac{c_{\mathrm{int},eq} c_{geom}}{c_{\mathrm{int},eq} + c_{geom}} \tag{40}$$

This low capacitance value is independent from the ionic concentration n_0, and the hole carrier injected density p_S, and it is the same than for an OMIS capacitor with $c_i = c_{int,eq}$[1] (dashed line in Figure 4a). For very negative voltages $V_{GS} << V_{FB}$ (strong accumulation regime), the capacitance tends asymptotically to a constant value, which is roughly equal (but slightly smaller) than the equivalent interfacial capacitance $c_{int,eq}$ (top red dot-dashed line in Figure 4a)

$$c_{GS,high} \approx c_{\mathrm{int},eq} \tag{41}$$

This value is also independent from both the ionic concentration n_0, and the injected hole density p_S, and again coincides with the value predicted for an OMIS capacitor with $c_i = c_{int,eq}$[1] (dashed line in Figure 4a). This asymptotic limit in the case of OMES is reached for much more negative voltages (not plotted in Figure 4) than for OMIS, which lie outside the operational voltage range of these devices (OMES are usually operated at voltages $V_{GS} > -1$ V). Therefore, OMES capacitors, contrary to OMIS capacitors, will typically not reach the strong accumulation regime, and hence will not display the high capacitance asymptotic value in Equation (41).

The moderate accumulation regime ($V_{GS} < V_{FB}$) covering the transition from the low to the high capacitance values $c_{GS,low}$ and $c_{GS,high}$, respectively, is relatively broad in an OMES capacitor and depends on both the ionic concentration of the electrolyte n_0, and the equivalent interfacial capacitance $c_{int,eq}$, while it is independent from the injected hole density p_S (compare continuous and dashed lines in Figure 4). The broadening of the transition is especially evident for low ionic concentrations ($n_0 < 10$ mM) and/or high interfacial capacitances ($c_{int,eq} > 10$ μF cm^{-2}).

To understand the broadening of the moderate accumulation range, we consider the distribution of the applied potential across the different parts of the capacitor,

$$V_{GS} = \Delta V_{ox,G} + \Delta V_{\mathrm{int}} + \Delta V_{sem} + \Delta V_{elec,G} + \Delta V_{elec,sem} \tag{42}$$

which includes the voltage drops across the compact interfacial layers at the gate/electrolyte and semiconductor/electrolyte interfaces, the semiconductor film and the two diffusive space charge layers at the gate/electrolyte and semiconductor/electrolyte interfaces. The overall device capacitance can be approximated by

$$c_{GS}{}^{-1} \approx c_{\mathrm{int},eq}{}^{-1} + \left[c_{sem}(V) + c_{geom}\right]^{-1} + 2c_{elec}(V)^{-1} \tag{43}$$

where we have introduced the voltage dependent diffusive capacitances of the ionic and hole space charge layers, respectively, defined as

$$c_{elec}(V) = \frac{\partial q_{elec,G}}{\partial \Delta V_{elec,G}} = \frac{\partial q_{elec,sem}}{\partial \Delta V_{elec,sem}}, c_{sem}(V) = \frac{\partial q_{sem}}{\partial \Delta V_{sem}} \tag{44}$$

For large negative voltages, one has $c_{sem}(V)$, $c_{sol}(V) >> 1$ due to the high density of free charges in the space charge layers, so Equation (43) predicts $c_{GS} \approx c_{int,eq} = c_{GS,high}$ as we have seen before. On the contrary, for large positive voltages $c_{sem}(V) << c_{geom}$, but still $c_{elec}(V) >> 1$, since for sufficiently positive voltages diffusive space charge layers also develop, Equation (43) predicts $c_{GS} \approx (c_{int,eq}{}^{-1} + c_{geom}{}^{-1})^{-1} = c_{GS,low}$, as, also, discussed before. Finally, in the transition from the weak to strong accumulation regimes both $c_{sem}(V)$ and $c_{elec}(V)$ play a role. The minimum value of $c_{sem}(V)$ is usually close to zero (it decays continuously for positive voltages), while that of $c_{elec}(V)$ is c_{elec} (Equation (19)), since $c_{elec}(V)$ increases for both positive and negative voltages. c_{elec} is typically of the order ≈5–10 μF cm^{-2}, even at low ionic concentrations. Therefore, the initial deviation of the capacitance from $c_{GS,low}$ is determined by $c_{sem}(V)$, as in the case of OMIS capacitors. This is the reason why the rising of the capacitance is well described by the OMIS model (see Figure 4), and it also explains why the flat-band potential V_{FB} is the same for OMES and OMIS. When the applied voltage becomes sufficiently negative $c_{sem}(V)$ becomes very high due to the injection of holes, and it overcomes c_{elec}. At this point, the transition starts being dominated by the ionic diffusive capacitance $c_{elec}(V)$, until this latter capacitance rises above $c_{int,eq}$, due to the accumulation of ions in the diffusive space charge layers, at which point the capacitance is dominated by $c_{int,eq}$, the equivalent interfacial compact layer capacitance. Accordingly, when $c_{int,eq} >> c_{elec}$ (i.e., for relatively low ionic concentrations, e.g. $n_0 < 100$ mM, and/or relatively high interfacial capacitances, e.g., $c_{int,eq} > 1$ μF cm^{-2}) the ionic diffusive capacitance $c_{elec}(V)$, plays an important role in the response of OMES capacitors and the OMIS model (or the Helmholtz approximation) does not correctly describe the physics of the device. In this case, the voltage dependence of $c_{elec}(V)$ gives rise to a broad transition between the weak and the strong accumulation regimes, as observed in Figure 4. Instead, if $c_{int,eq} << c_{elec}$ (i.e., high ionic concentrations, e.g. $n_0 > 100$ mM, and/or relatively low interfacial capacitances, e.g. $c_{int,eq} < 1$ μF cm^{-2}) one has that $c_{elec}(V)$ practically does not play any role in any voltage range, and the system can be described neglecting the ionic diffusive effects, that is, by means of the Helmholtz approximation (or the OMIS theory). Finally, Figure 4c confirms that the "flat-band" voltage V_{FB} defined in Equation (35) indeed correctly predicts the voltage at which the capacitance starts deviating from the low capacitance value. We verified it by determining the shifts of the capacitance curves with respect to the curve for p_S^* and comparing them with the prediction of Equation (35) (symbols and continuous line, respectively, in the inset in Figure 4c). The agreement is perfect.

For completeness we have also analyzed the voltage dependence of the sheet charge accumulated in the semiconductor film q_{sem}, since it is a magnitude relevant to understand the physics of, for instance, EGOFETs. **Figure 5**a–c shows the dependence on the source-gate voltage V_{GS} of the sheet semiconductor charge q_{sem} for different ionic concentrations of the electrolyte n_0, equivalent interfacial capacitances $c_{int,eq}$, and injected hole densities p_S, respectively. The sheet semiconductor charge has been calculated from Equation (30), with the values of β obtained by solving Equations (22) and (23). The predictions of the OMIS theory for $c_i = c_{int,eq}$ has been plotted as dashed lines. They have been obtained by evaluating the parametric analytical expression given by Equations (30) and (32). The insets in Figure 4 represent the same data than in the main panel but plotted in log-linear representation. In the weak accumulation regime ($V_{GS} > V_{FB}$), the sheet semiconductor charge q_{sem} shows an initial exponential decay followed by a slower inverse decay, as predicted by Equation (38). On the other hand, in the strong accumulation regime ($V_{GS} >> V_{FB}$) q_{sem} tends to increase apparently "linearly" with the applied gate voltage, although the dependence is not strictly linear. A true linear dependency is only attained for very negative voltages (not shown), which lie outside the physical voltage range of operation of OMES. On the contrary, in the case of OMIS capacitors (or in the case of OMES capacitors in the Helmholtz approximation) the charge follows a nice linear dependency for moderate values of the applied voltage (dot-dashed line). In this case, the response can be approximated by Equation (39). The lack of a strict linear dependence of q_{sem} with the source-gate voltage V_{GS} in the case of OMES makes ambiguous the definition of the threshold voltage V_{TH} and of the device phenomenological capacitance c_{DL} appearing in Equation (39), what can have important implications (see below). Instead, in the case of OMIS capacitors, since the relationship between q_{sem} and V_{GS} is linear, Equation (39) applies, and c_{DL} and V_{TH} can be readily defined and extracted in an unambiguous way (dot-dashed line in Figure 5a).

Finally, in the moderate accumulation regime ($V_{GS} < V_{FB}$) q_{sem} shows an evolution from an exponential dependency to the quasi-linear dependency mentioned above. The most relevant property of this regime is that it is much broader than for the case of OMIS capacitors, due to the role played by the ionic diffusive space charge layers in the electrolyte, especially for low ionic concentrations and/or high interfacial compact capacitances, as discussed before.

4. Discussion

We have presented the stationary analytical physical modeling of undoped OMES capacitors in the framework of the NPP theory with the presence of compact interfacial layers (equivalent to the Stern–Gouy–Chapman solid/electrolyte theory). This physical model includes the presence of ionic diffusive effects in the electrolyte, which are not present in the models of OMIS capacitors,[1] or when the Helmholtz approximation is considered OMES capacitors. The main findings of the analysis presented can be summarized in the following points:

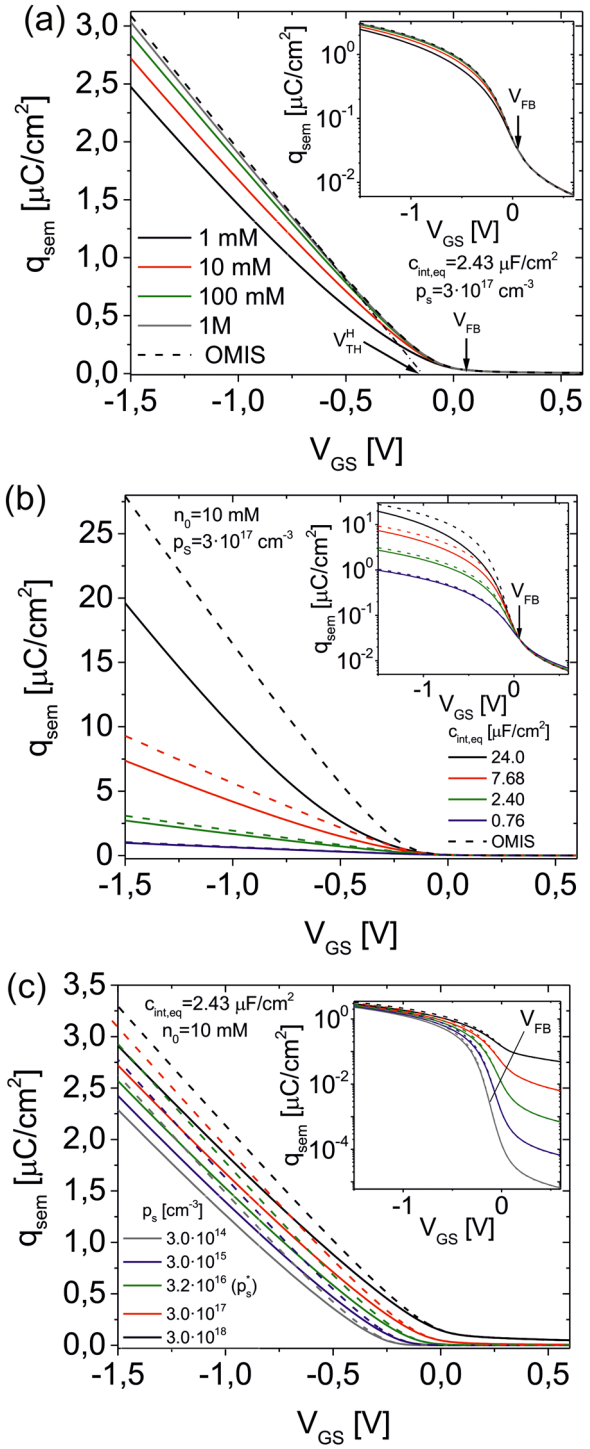

Figure 5. Sheet semiconductor charge, q_{sem}, as a function of the source gate voltage, V_{GS}, for different a) ionic concentration of the electrolyte, n_0, b) equivalent interfacial capacitances, $c_{int,eq}$ and c) injected hole density, p_S. The dashed lines represent the predictions obtained in the Helmholtz approximation with $c_H = c_{int,Equation}$ The insets represent the same data plotted in log-linear representation. Parameters: same as in Figure 3, unless otherwise stated: $\epsilon_{sem} = 4$, $\epsilon_{elec} = 78$, $n_0 = 10$ mM, $h_{sem} = 30$ nm, $h_{elec} = 100$ μm, $c_G = 7.3$ μF cm^{-2}, $c_{int} = 3.65$ μF cm^{-2} ($c_{int,eq} = 2.43$ μF cm^{-2}), $q_{fix,G} = 0$ C m^{-2}, $p_S = 3{\cdot}10^{17}$cm^{-3}. For these parameters, $c_{geom} = 0.12$ μF cm^{-2}.

i. OMES capacitors, as well as OMIS capacitors, show a voltage dependent capacitance, which is limited by two asymptotic capacitance values, namely, $c_{GS,low}$ and $c_{GS,high}$, given by Equations (40) and (41), respectively. The low capacitance value is given by the series combination of the equivalent interfacial compact capacitance $c_{int,eq}$ and the geometric semiconductor capacitance c_{geom}. The high capacitance value depends solely on $c_{int,eq}$ In the case of OMES capacitors, the high capacitance value may not be reachable within the operational voltage range of the capacitors since it is attained at very large negative voltages not compatible with the operation in electrolytes (see below).

ii. The capacitance of the compact interfacial layers associated to the Stern layers or to other types of ultrathin layers (e.g., functionalization biolayers, phase separated material layers, etc.) play a fundamental role in the device response, and their effects cannot be neglected. Stern layers associated to the adsorption of ions, water molecules, contaminants, etc., typically show high interfacial capacitances (>10's μF cm^{-2}), while interfacial layers associated to the presence of functionalization layers or to phase separated material layers tend to present smaller interfacial capacitance values (<1 μF cm^{-2}). These capacitance values, even if high, are much smaller than the values that the ionic and hole diffusive capacitances can reach for large (negative) source-gate voltages. Therefore, the compact interfacial capacitances ultimately govern the response of the capacitor in the strong accumulation regime, and this is the reason why they determine the value of the high capacitance asymptotic value. In the absence of interfacial capacitances, the capacitance and the sheet accumulated charge would increase exponentially in an unbounded (and unphysical) way, as it happens in the Gouy–Chapman theory.

iii. Ionic diffusive effects can play a relevant role in the voltage dependence of the capacitance of OMES capacitors. Ionic diffusive effects consist in the formation of ionic diffusive space charge layers at the gate/electrolyte and semiconductor/electrolyte interfaces, whose capacitance is voltage dependent. As a result, the transition from the weak to the strong accumulation regimes (moderate accumulation regime) broadens significantly. In the absence of ionic diffusive effects (when the Helmholtz approximation holds or for the case of OMIS capacitors) the moderate accumulation regime is quite narrow and the transition to the high capacitance value quite sharp. However, when ionic diffusive effects play a relevant role, the moderate accumulation regime expands several 100's mV. Then, it can comprise the whole operational voltage range of the capacitor (OMES capacitors most often cannot be biased for voltages larger than ±1 V in order to avoid the occurrence of irreversible electrochemical effects). Ionic diffusive effects are mostly relevant for low ionic concentrations (n_0 < 100 mM) and/or high interfacial capacitances ($c_{int,eq}$ > 1 μF cm^{-2}).

iv. A "flat-band" potential V_{FB}, determining the departure of the capacitance from the low capacitance value, has been identified (Equation (35)) by using the characteristic injected hole density p_S^*(Equation (34)). This potential does not imply that the potential in the semiconductor is flat, since in undoped semiconductor devices this never happens. The "flat- band" potential depends on the fixed charges present at the elec-

trolyte/gate (and /semiconductor) interfaces and on the level of injected carriers, p_S (and on the difference in metal work functions when present). Therefore, the flat-band potential is independent from the presence of ionic diffusive effects, and hence it is the same than for OMIS capacitors.

The NPP model considered here could be complemented by including additional effects or phenomena such as semiconductor degeneracy effects,[1] ionic–ionic interactions and finite-size ionic effects,[13,14] the presence of unintentional doping, bulk fixed charges and ionic conductivity in the compact interfacial layers for biosensor modeling,[15] ionic permeability of the semiconductor film, polarization of the source/semiconductor interface, the presence of disorder, non 1D geometries, minority carriers, etc. In most of these cases, an analytical solution cannot be obtained, and one must resort to numerical solutions of the problems. Still, the essential aspects of the physics of OMES capacitors are expected to be captured by the theory presented here.

The frequency response of the device has not been analyzed, here, as only stationary (low frequency) properties have been described. The strong frequency dependence of ionic diffusive layers is expected to lead to complex frequency dependencies and to a further departure of the behavior of OMES capacitors with respect to OMIS capacitors.[16,17] The analysis of the frequency dependency has been carried out by means of equivalent circuit models.[16,17] The development of an analytical physical theory based on the NPP framework to describe them lies outside the scope of the present work and will be considered in future works.

The comparison of the voltage dependence of the capacitance predicted by the theory presented here with experimental results can be performed only at a qualitative level, due to the lack of systematic experimental measurements performed directly on OMES capacitor structures. While the frequency dependency has been analyzed in some detail, as mentioned above,[16,17] the voltage dependence has been scarcely considered in detail.[18,19] There exist some capacitance measurements performed on EGOFETs (for instance in ref. [20]), which can provide additional insight, although a quantitative comparison is more complicated since both the electrodes and channel regions contribute to the measured capacitance, making difficult to separate the different contributions. In any case, the general trend of the capacitance–voltage characteristic curves measured on OMES capacitors (or on EGOFETs) show the characteristic trend described by the theory, but more experiments (e.g., by varying the ionic concentration, using functionalization layers, etc.) would be necessary to asses it against the simpler OMIS capacitor theory.

Finally, we note that the results presented here can have some relevant implications regarding the physics of EGOFETs. The most relevant implication is that ionic diffusive effects can make that the linear relationship between the sheet semiconductor charge q_{sem} and the source-gate voltage V_{GS} (Equation (39)), usually assumed in the modeling of EGOFETs, breaks down within the voltage range of operation of these devices. Therefore, the ideal quadratic Thin-Film-Transistor FET I-V characteristics model usually used to describe EGOFETs may not hold.[21] Consequently, the definition and extraction of phenomenological parameters like the threshold voltage V_{TH} or the device capacitance c_{DL} may become ambiguous and dependent on the extraction conditions (e.g., voltage range considered). This ambiguity can be especially relevant in the case of EGOFET biosensors,[8] whose response is conventionally interpreted in terms of TFT like models and parametrized through the extraction of its phenomenological parameters. Further work is necessary to determine how severe this limitation may be. On the other hand, when ionic diffusive effects can be neglected, we have shown that the Helmholtz approximation can be used to describe OMES capacitors, and hence, it is also expected to hold in the description of EGOFETs. An analytical theory for EGOFETs in the Helmholtz approximation has been recently derived in ref. [22].

5. Conclusions

In summary, we have analyzed theoretically the static characteristics of OMES capacitors in the framework of the NPP theory, including the presence of ultrathin interfacial compact layers. An analytical solution to the model has been derived and validated by means of finite-element numerical calculations. Results indicate that the ionic diffusive space charge layers, and its voltage dependence, can play a relevant role for low/medium ionic concentrations and/or large equivalent compact interfacial capacitances, thus making necessary its explicit consideration into the models. Similarly, the presence of the ultrathin compact interfacial layers also needs to be considered in order to avoid an unbounded increase of the ionic diffusive capacitance and of the hole accumulated density in the semiconductor. The Helmholtz approximation, or the OMIS theory, has been shown to apply only when thes ionic diffusive effects can be neglected. The results presented here shed some new light into the physics of electrolyte gated organic devices, such as EGOFETs, which could contribute to its better understanding and quantitative characterization.

Appendix A: Derivation of the Analytical Solution

In this appendix we present the derivation of the analytical solution in Equations (14) and (15). Since the fixed interfacial charge at the gate/electrolyte interface, $q_{fix,G}$, just adds an offset, ΔV_{qfix} to the source-gate voltage, V_{GS}, (see Equations (9) and (10)), its effect will be added explicitly only in the final expressions after solving the model for $q_{fix,G} = 0$. Under stationary conditions, and given the one dimensionality of the problem, the ions and hole fluxes, $J_{\pm}(z)$ and $J_p(z)$, respectively, are constant (see Equations (2) and (5)). Moreover, the zero flux boundary conditions (Equations (8)) imply that the constants have to be 0, that is, $J_{\pm}(z) = 0$ and $J_p(z) = 0$. The null current conditions imply that the electrochemical potentials of both the ions and the holes are constant in the electrolyte and semiconductor, respectively. Indeed, if we introduce the chemical potentials of the holes and ions for non-degenerate and dilute systems, respectively, through the usual relationships.

$$\tilde{\mu}_p = \tilde{\mu}_{p_S} + k_B T \ln\left(\frac{p}{p_S}\right) \tag{A1}$$

$$\tilde{\mu}_{\pm} = \tilde{\mu}_{n_0} + k_B T \ln\left(\frac{n_{\pm}}{n_0}\right) \tag{A2}$$

where $\tilde{\mu}_{p_S}$ and $\tilde{\mu}_{n_0}$ are the chemical potentials of reference associated to the concentrations p_S and n_0, and then define the electrochemical potentials as

$$\phi_p = \tilde{\mu}_p + e\varphi \tag{A3}$$

$$\phi_{\pm} = \tilde{\mu}_{\pm} \pm e\varphi \tag{A4}$$

it is immediate to show from Equations (3) and (6) that the electrochemical potentials ϕ_p and $\phi_\pm$ are constant in space. In the semiconductor field, the chemical potentials are referred to as the Fermi levels and the electrochemical potentials as the quasi-Fermi levels. From Equations (A1)–(A4) the carrier densities can be written in a Boltzmann-like distribution form

$$p = p_S \exp\left(\frac{\phi_p - \tilde{\mu}_{p_S}}{k_B T}\right) e^{-\frac{e\varphi_{sem}}{k_B T}} \tag{A5}$$

$$n_\pm = n_0 \exp\left(\frac{\phi_\pm - \tilde{\mu}_{n_0}}{k_B T}\right) e^{\mp\frac{e\varphi_{elec}}{k_B T}} \tag{A6}$$

For non-zero source-gate potentials, the electrochemical potentials of the different species, ϕ_p and $\phi_\pm$, differ from each other. Determining their values as a function of the applied voltage is part of finding the solution to the problem. The chemical potential of the holes can also be defined in terms of the density of states in the semiconductor and the energy of the Highest Occupied Molecular Orbital (HOMO), when these concepts apply. In that case, instead of Equation (A1), one would have

$$\tilde{\mu}_p = \tilde{\mu}_{HOMO} + k_B T \ln\left(\frac{p}{N_{HOMO}}\right) \tag{A7}$$

from where

$$\tilde{\mu}_{p_S} = \tilde{\mu}_{HOMO} + k_B T \ln\left(\frac{p_S}{N_{HOMO}}\right) \tag{A8}$$

By substituting Equations (A5) and (A6) into Poisson's equations (Equations (1) and (4)) one arrives at,

$$\frac{d^2\tilde{\varphi}_{sem}}{dz^2} = -\frac{e\tilde{p}_S}{\varepsilon_0\varepsilon_{sem}} \exp\left(-\frac{e\tilde{\varphi}_{sem}}{k_B T}\right), z_S \le z \le z_{\text{int}}^- \tag{A9}$$

$$\frac{d^2\tilde{\varphi}_{elec}}{dz^2} = 2\frac{e\tilde{n}_0}{\varepsilon_0\varepsilon_{elec}} \sinh\left(\frac{e\tilde{\varphi}_{elec}}{k_B T}\right), z_{\text{int}}^+ \le z \le z_G^- \tag{A10}$$

where we have introduced the effective electric potential as

$$e\tilde{\varphi} = e\varphi - \Delta\phi \tag{A11}$$

and the difference and mean electrochemical potentials as

$$\Delta\phi = \frac{\phi_+ - \phi_-}{2} \tag{A12}$$

$$\bar{\phi} = \frac{\phi_+ + \phi_-}{2} \tag{A13}$$

Moreover, we have introduced the effective carrier densities

$$\tilde{n}_0 = n_0 \exp\left(\frac{\bar{\phi} - \tilde{\mu}_{n_0}}{k_B T}\right) \tag{A14}$$

$$\tilde{p}_S = p_S \exp\left(\frac{\phi_p - \tilde{\mu}_{p_S} - \Delta\phi}{k_B T}\right) \tag{A15}$$

As usual, a first integration of Equations (A9) and (A10) can be made by multiplying these equations by the derivative of the electric potential and integrating afterward. One obtains

$$\frac{d\tilde{\varphi}_{sem}}{dz} = \pm\sqrt{\frac{2k_B T\tilde{p}_S}{\varepsilon_0\varepsilon_{sem}}\left[e^{-\frac{e\tilde{\varphi}_{sem}}{k_B T}} - e^{-\frac{e\tilde{V}_S}{k_B T}}\right] + \left(\frac{d\tilde{\varphi}_S}{dz}\right)^2}, \; z_S \le z \le z_{\text{int}}^- \tag{A16}$$

$$\frac{d\tilde{\varphi}_{elec}}{dz} = \pm\sqrt{\frac{4k_B T\tilde{n}_0}{\varepsilon_0\varepsilon_{sol}}\left(\cosh\left[\frac{e\tilde{\varphi}_{elec}}{k_B T}\right] - \cosh\left[\frac{e\tilde{\varphi}_G^-}{k_B T}\right]\right) + \left(\frac{d\tilde{\varphi}_G^-}{dz}\right)^2},$$

$$z_{\text{int}}^+ \le z \le z_G^- \tag{A17}$$

Note that two pairs of $\pm$ signs appear, which we have drawn in different colors (red and blue) to be distinguished. Equation (A16) can be integrated again, while Equation (A17) can be reduced to a quadrature,

$$\frac{e\tilde{\varphi}_{sem}(z)}{k_B T} = -\ln\left\{a\tan^2\left[\mp\frac{(z - z_S)}{2\tilde{L}_{Ds}}\sqrt{a} + \tan^{-1}\left(\frac{\sqrt{e^{-\frac{e\tilde{V}_S}{k_B T}} - a}}{\sqrt{a}}\right)\right] + a\right\},$$

$$z_S \le z \le z_{\text{int}}^- \tag{A18}$$

$$z - z_G = \pm\tilde{L}_D \int_{\frac{e\tilde{\varphi}_G^-}{k_B T}}^{\frac{e\tilde{\varphi}_{elec}(z)}{k_B T}} \frac{d\gamma}{\sqrt{2\cosh(\gamma) - b}}, z_{\text{int}}^+ \le z \le z_G^- \tag{A19}$$

Here, we have introduced the effective Debye screening lengths

$$\tilde{L}_D = \sqrt{\frac{k_B T\varepsilon_0\varepsilon_{elec}}{2e^2\tilde{n}_0}}, \tilde{L}_{Ds} = \sqrt{\frac{k_B T\varepsilon_0\varepsilon_{sem}}{2e^2\tilde{p}_S}} \tag{A20}$$

and the auxiliary parameters

$$a = e^{-\frac{e\tilde{V}_S}{k_B T}} - \left(\frac{d\tilde{\varphi}_S}{dz}\right)^2\left(\frac{e\tilde{L}_{Ds}}{k_B T}\right)^2 \tag{A21}$$

$$b = 2\cosh\left[\frac{e\tilde{\varphi}_G^-}{k_B T}\right] - \left(\frac{d\tilde{\varphi}_G^-}{dz}\right)^2\left(\frac{e\tilde{L}_D}{k_B T}\right)^2 \tag{A22}$$

To determine the solution of the problem one needs to determine the derivatives $d\tilde{\varphi}_S/dz$ and $d\tilde{\varphi}_G/dz$ (or equivalently the parameters a and b), the potential, $\tilde{\varphi}_G$ and the electrochemical potentials ϕ_p, $\bar{\phi}$, and $\Delta\phi$. To this end, we apply the boundary and continuity conditions.

The hole electrochemical potential ϕ_p can be determined by imposing in Equation (A5) the boundary conditions in Equations (7) and (13). One simply obtains

$$\phi_p = \tilde{\mu}_{p_S} - eV_S \tag{A23}$$

Note, that the diffusive boundary condition implies that $\phi_p = \phi_S$, where ϕ_S is the electrochemical potential of the source electrode. This fact, together with the non-polarizable nature of the interface, implies that the chemical potential related to the hole injection density equals the Fermi level of the source $\tilde{\mu}_{p_S} = E_{F,S}$. In terms of the density of states this result implies that (see Equation (A8))

$$p_S = N_{HOMO} \exp\left(-\frac{e\phi_{bp}}{k_B T}\right), \tag{A24}$$

where $e\phi_{bp} = \tilde{\mu}_{HOMO} - E_{F,S}$ is the barrier height for hole injection, which in a simple Mott–Schottky approximation is given by the difference between the hole ionization energy and the source metal work function, that is, $e\phi_{bp} = IE_p - \phi_{m,S}$.

On the other hand, the zero flux boundary conditions at the two interfaces of the electrolyte imply that total number of ions in the electrolyte is constant. This constant value is given by

$$N_{\pm} = n_0 \left(z_G - z_{\text{int}}\right) = \int_{z_{\text{int}}^{+}}^{z_G^{-}} n_{\pm} dz \tag{A25}$$

By subtracting them, one obtains

$$N_{+} - N_{-} = 0 = \int_{z_{\text{int}}^{+}}^{z_G^{-}} \left(n_{+} - n_{-}\right) dz \tag{A26}$$

The right-hand side of Equation (A26) can be integrated by using Poisson's equation, Equation (4), to give

$$\frac{d\varphi_G^{-}}{dz} - \frac{d\varphi_{\text{int}}^{+}}{dz} = 0 \tag{A27}$$

By evaluating Equation (A17) at $z_{int}{}^{+}$ and using Equations (A11) and (A27) one obtains

$$\tilde{\varphi}_{\text{int}}^{+} = -\tilde{\varphi}_G^{-}, \tag{A28}$$

or equivalently

$$\frac{\Delta\phi}{e} = \frac{\varphi_{\text{int}}^{+} + \varphi_G^{-}}{2} \tag{A29}$$

On the other side, by adding up the carrier concentrations in Equation (A25) one obtains

$$N_{+} + N_{-} = 2n_0 \left(z_G - z_{\text{int}}\right) = \int_{z_{\text{int}}^{+}}^{z_G^{-}} \left(n_{+} + n_{-}\right) dz, \tag{A30}$$

which by using Equations (A6), (A11), and (A13) transforms into

$$\exp\left(-\frac{\bar{\phi} - \tilde{\mu}_{n_0}}{k_B T}\right) = \frac{1}{h_{elec}} \int_{z_{\text{int}}^{+}}^{z_G^{-}} \cosh\left(\frac{e\tilde{\varphi}_{elec}}{k_B T}\right) dz, \tag{A31}$$

where we have used that $z_G - z_{\text{int}} = h_{elec}$. By making the change of variables $\gamma = e\tilde{\varphi}/k_B T$ and using Equation (A17), (A22), and (A28) we arrive at

$$\exp\left(-\frac{\bar{\phi} - \tilde{\mu}_{n_0}}{k_B T}\right) = \mp\frac{2\tilde{L}_D}{h_{elec}} \int_{0}^{\frac{e\tilde{\varphi}_G^{-}}{k_B T}} \frac{\cosh\left(\gamma\right)}{\sqrt{2\cosh\left(\gamma\right) - b}} d\gamma \tag{A32}$$

Finally, by using Equations (A14) and (A20) we obtain

$$\exp\left(-\frac{\bar{\phi} - \tilde{\mu}_{n_0}}{2k_B T}\right) = \mp\frac{2L_D}{h_{elec}} \int_{0}^{\frac{e\tilde{\varphi}_G^{-}}{k_B T}} \frac{\cosh\left(\gamma\right)}{\sqrt{2\cosh\left(\gamma\right) - b}} d\gamma, \tag{A33}$$

where we have introduced the Debye screening length of the electrolyte, L_D, as in Equation (20).

We now impose the continuity of the displacement field at the semiconductor/electrolyte interface, Equation (12). To do so, we use the expressions for the derivatives of the electric potential in Equations (A16) and (A17), and the definitions of the parameters a and b in Equations (A21) and (A22). One arrives at the relation

$$2\cosh\left[\frac{e\tilde{\varphi}_G^{-}}{k_B T}\right] - b = \left(\frac{c_{sem}}{c_{elec}}\right)^2 \left(\frac{\tilde{L}_D}{L_D}\frac{L_{Ds}}{\tilde{L}_{Ds}}\right)^2 \left(\exp\left(\frac{e\tilde{\varphi}_G^{-}}{k_B T} \pm \frac{c_{elec}}{c_{\text{int}}}\left(\frac{L_D}{\tilde{L}_D}\right)\sqrt{2\cosh\left[\frac{e\tilde{\varphi}_G^{-}}{k_B T}\right] - b}\right) - a\right) \tag{A34}$$

where use has been made of Equations (11) and (A28). Here we have introduced the specific diffusive capacitances of the electrolyte and semiconductor c_{elec} and c_{sem}, respectively, as defined in Equation (19) and the Debye screening length of the semiconductor L_{Ds} as in Equation (20).

On the other hand, we impose the discontinuity in the potential at the semiconductor/electrolyte interface (Equation (11)). To this end, we first determine from Equation (A18) the potential at the semiconductor/electrolyte interface

$$\frac{e\tilde{\varphi}_{\text{int}}^{-}}{k_B T} = -\ln\left\{a\tan^2\left[\mp\frac{h_{sem}\sqrt{a}}{2\tilde{L}_{Ds}} + \tan^{-1}\left(\frac{\sqrt{e^{-\frac{e\tilde{V}_S}{k_B T}} - a}}{\sqrt{a}}\right)\right] + a\right\}, \tag{A35}$$

where we have used that $z_{\text{int}} - z_S = h_{sem}$. Then, from Equations (11), (19), (A17), and (A22) we obtain

$$\frac{e\tilde{\varphi}_{\text{int}}^{-}}{k_B T} = \frac{e\tilde{\varphi}_{\text{int}}^{+}}{k_B T} \mp \frac{c_{elec}}{c_{\text{int}}}\left(\frac{L_D}{\tilde{L}_D}\right)\sqrt{\left(2\cosh\left[\frac{e\tilde{\varphi}_{\text{int}}^{+}}{k_B T}\right] - b\right)} \tag{A36}$$

By equating Equations (A35) and (A36) we obtain

$$\frac{-e\tilde{\varphi}_G^{-}}{k_B T} \mp \frac{c_{elec}}{c_{\text{int}}}\left(\frac{L_D}{\tilde{L}_D}\right)\sqrt{\left(2\cosh\left[\frac{e\tilde{\varphi}_G^{-}}{k_B T}\right] - b\right)} = -\ln\left\{a\tan^2\left[\mp\frac{h_{sem}\sqrt{a}}{2\tilde{L}_{Ds}} + \tan^{-1}\left(\frac{\sqrt{e^{-\frac{e\tilde{V}_S}{k_B T}} - a}}{\sqrt{a}}\right)\right] + a\right\}, \tag{A37}$$

where we used Equation (A28). Finally, we impose the boundary condition at the gate electrode, Equation (9). By using in it Equations (A21) and (A22), which relate the derivatives of the electric potential to the parameters a and b, we arrive at

$$\frac{e\tilde{\varphi}_G^{-}}{k_B T} = \frac{e\tilde{V}_G}{k_B T} \mp \frac{c_{elec}}{c_G}\frac{L_D}{\tilde{L}_D}\sqrt{2\cosh\left[\frac{e\tilde{\varphi}_G^{-}}{k_B T}\right] - b} \tag{A38}$$

By combining Equations (A34) and (A38) we can write an alternative expression

$$\frac{e\tilde{\varphi}_G^{-}}{k_B T} = \frac{e\tilde{V}_G}{k_B T} \mp \frac{c_{sem}}{c_G}\frac{L_{Ds}}{\tilde{L}_{Ds}}\sqrt{\exp\left[\left(1 - \frac{c_G}{c_{\text{int}}}\right)\frac{e\tilde{\varphi}_G^{-}}{k_B T} + \frac{c_G}{c_{\text{int}}}\frac{e\tilde{V}_G}{k_B T}\right] - a} \tag{A39}$$

With this step we completed the derivation of the analytical solution of the problem. To render the final expressions as in Equations (14) and (15), we introduced some changes of variables. First, we introduce the parameters f and f' as

$$f \equiv \frac{\tilde{L}_D}{L_D} = \exp\left(\frac{\tilde{\mu}_{n_0} - \bar{\phi}}{2k_B T}\right), f' \equiv \frac{\tilde{L}_{Ds}}{L_{Ds}} = \exp\left(-\frac{e\tilde{V}_S}{2k_B T}\right), \tag{A40}$$

and then the parameters β and $\tilde{\alpha}$ as

$$\tilde{\alpha} = \frac{1}{af'^2} \exp\left[\frac{e\left(\tilde{V}_G - \tilde{V}_S\right)}{k_B T}\right], \beta = \frac{a}{f'^2} \tag{A41}$$

With these definitions it can be shown that Equations (A39) and (A41) read

$$\frac{e\varphi_G^-}{k_B T} = \frac{eV_G}{k_B T} \pm \frac{c_{sem}}{c_G}\sqrt{\beta\,(\alpha - 1)}, \tag{A42}$$

$$\tilde{\alpha} = \alpha \exp\left[\left(\frac{c_{sem}}{c_{\text{int}}} - \frac{c_{sem}}{c_G}\right)\sqrt{\beta\,(\alpha - 1)}\right], \tag{A43}$$

where we have defined α as in Equation (18). By using these changes of variables in Equations (A18) and (A19), and after some algebra, the solution for the electric potential can be written as in Equations (14) and (15), with the definitions in Equations (16)–(18). Moreover, Equations (A31) and (A33) can be written in terms of the parameters f and β as in Equations (22) and (23).

To evaluate Equation (15) it is worth having the limiting values for the potential in the electrolyte region. They are given by φ_G^- in Equation (A42) and by

$$\frac{e\varphi_{\text{int}}^+}{k_B T} = \frac{eV_S}{k_B T} \mp \frac{c_{sem}}{c_{\text{int}}}\sqrt{\beta\,(\alpha - 1)} - \ln(\alpha\beta) \tag{A44}$$

The charge density in the semiconductor can be calculated from the electric potential as

$$\rho_{sem}(z) = ep(z) = ep_S e^{-\frac{e[\varphi_{sem}(z) - V_S]}{k_B T}}, \tag{A45}$$

which is obtained by combining Equations (A5) and (A23). By substituting Equation (14) in Equation (A45), and using that $1+\tan^2(x) = 1/\cos^2(x)$, one obtains Equation (26). For the charge density in the electrolyte, by using Equations (A6) and the definitions in Equations (A12) and (A13), one has

$$\rho_{sol}(z) = -2en_0 \exp\left(\frac{\bar{\phi} - \tilde{\mu}_0}{k_B T}\right)\sinh\left(\frac{e\varphi_{sol}(z) - \Delta\phi}{k_B T}\right) \tag{A46}$$

By using Equations (17), (A40), (A41), and (A43) in it one finally obtains Equation (27).

The charge accumulated at the source electrode can be obtained as

$$q_S = -\varepsilon_0 \varepsilon_{sem}\frac{d\varphi_S}{dz} \tag{A47}$$

By using Equation (14) to calculate the derivative one obtains Equation (28). For the gate electrode we similarly have

$$q_G = \varepsilon_0 \varepsilon_{elec}\frac{d\varphi_G^-}{dz} + q_{fix,G} =$$

$$\varepsilon_0 \varepsilon_{elec}\frac{d\varphi_{\text{int}}^+}{dz} + q_{fix,G} = \varepsilon_0 \varepsilon_{sem}\frac{d\varphi_{\text{int}}^-}{dz} + q_{fix,G}, \tag{A48}$$

where use has been made of the continuity of the displacement field through the different dielectric interfaces and of the relation in Equation (A27). By using again Equation (14) to calculate the derivative on the right-hand side of Equation (A48) and the definition in Equation (18) one obtains Equation (29). Finally, the charge accumulated across the semiconductor film per unit of area is given by

$$q_{sem} = \int_{z_S}^{z_{\text{int}}} ep(z)\,dz = -\varepsilon_0 \varepsilon_{sem}\left[\frac{d\varphi_{\text{int}}^-}{dz} - \frac{d\varphi_S^+}{dz}\right] =$$

$$-q_G + q_{\text{int},G} - q_S, \tag{A49}$$

as it should be by charge conservation. By using Equations (28) and (29) one obtains Equation (30).

Table 1. Sign convention for the analytical expressions.

Red Sign	Bottom	Upper	Upper	Bottom
Blue Sign	Bottom	Bottom	Upper	Upper
		$p_S^* \le p_S$		
β	$(-\infty, 0]$	$[0, \beta_1]$	$[\beta_1, \beta_2)$	–
		$\frac{4}{\pi^2}p_S^* \le p_S \le p_S^*$		
β	–	$(-\infty, 0]$	$[0, 1]$	$[1, \beta_3)$
		$p_S \le \frac{4}{\pi^2}p_S^*$		
β	$(-\infty, 0]$	$[0, \beta_1]$	$[\beta_1, 1] \cup (\beta_4, 0]$	$[0, 1]$

Appendix B: Sign Convention

In the derivation of the analytical solution there appear two independent pairs of ± signs (represented in red and blue colors). Therefore, in general, there are four possible combinations of signs. The actual combination of signs depends on the value of the parameter β. We have found that to a good approximation, the sign convention is the same than the one found in the analysis of the solution in the Helmholtz approximation, which is much simpler to analyze. We summarize the results obtained for the sign convention in **Table 1**.

The parameters β_1, β_2, β_3, and β_4 appearing in Table 1 are, respectively, the solutions of the following equations

$$\begin{aligned}
&\frac{h_{sem}}{2L_{Ds}}\sqrt{\beta_1} - \tan^{-1}\left(\sqrt{\frac{1}{\beta_1} - 1}\right) = 0,\\
&\frac{h_{sem}}{2L_{Ds}}\sqrt{\beta_2} - \tan^{-1}\left(\sqrt{\frac{1}{\beta_2} - 1}\right) = \frac{\pi}{2},\\
&\frac{h_{sem}}{2L_{Ds}}\sqrt{\beta_3} + \tan^{-1}\left(\sqrt{\frac{1}{\beta_3} - 1}\right) = \frac{\pi}{2},\\
&\frac{h_{sem}}{2L_{Dsem}}\sqrt{|\beta_4|} + \frac{1}{2}\ln\left(\frac{\sqrt{\frac{1}{|\beta_4|} + 1} - 1}{\sqrt{\frac{1}{|\beta_4|} + 1} + 1}\right) = 0,
\end{aligned} \tag{B1}$$

with p_S^* given in Equation (35).

Appendix C: Real Analytical Expressions for $\beta < 0$.

The solution for the electric potential in the semiconductor in Equation (14) for $\beta < 0$ can be written in terms of real functions as

$$\frac{e[\varphi_{sem}(z) - V_S]}{k_B T} = -\ln\left\{|\beta|\coth^2\left[\pm\frac{(z - z_S)}{2L_{Ds}}\sqrt{|\beta|} + \frac{1}{2}\ln\left(\frac{\sqrt{\frac{1}{|\beta|} + 1} - 1}{1 + \sqrt{\frac{1}{|\beta|} + 1}}\right)\right] - |\beta|\right\}, \quad z_S \le z \le z_{\text{int}} \tag{C1}$$

Moreover, the function α in Equation (18) can be written as

$$\alpha = 1 - \coth^2\left[\pm\frac{h_{sem}}{2L_{Ds}}\sqrt{|\beta|} + \frac{1}{2}\ln\left(\frac{\sqrt{\frac{1}{|\beta|}+1}-1}{1+\sqrt{\frac{1}{|\beta|}+1}}\right)\right] \tag{C2}$$

The remaining functions are directly real for $\beta < 0$. To arrive at these expressions, we used the following relationships valid in the complex plane

$$\cot(ix) = i\coth(x),\ \tan^{-1}(x) = \frac{1}{2i}\ln\left(\frac{i-x}{i+x}\right),$$

$$\ln(-1) = i\pi,\ \tan\left(x+\frac{\pi}{2}\right) = -\cot(x), \tag{C3}$$

$$\coth\left[\ln\left(x^{1/2}\right)\right] = \frac{\left(x^{1/2}\right)^2+1}{\left(x^{1/2}\right)^2-1} = \frac{x+1}{x-1} \tag{C3}$$

Appendix D: Expressions in Terms of Incomplete Elliptic Integrals

Equations (22) and (23) can be expressed in terms of incomplete elliptic integrals of the first and second kind, *F[ϕ,k]* and *E[ϕ,k]*, respectively, as

$$\pm\frac{h_{elec}}{2L_D}\frac{\sqrt{2-b(\beta,f)}}{2f} = iF\left[i\frac{e\Delta\varphi_{elec}(\beta)}{4k_BT}, \frac{2}{\sqrt{2-b(\beta,f)}}\right] \tag{D1}$$

$$\pm\frac{h_{elec}}{2L_D}\frac{\left(f-\frac{b(\beta,f)}{2f}\right)}{\sqrt{2-b(\beta,f)}} = iE\left[i\frac{e\Delta\varphi_{elec}(\beta)}{4k_BT}, \frac{2}{\sqrt{2-b(\beta,f)}}\right] \tag{D2}$$

where the elliptic integrals are defined as

$$E(\phi,k) = \int_0^{\phi}\sqrt{1-k^2\sin^2\theta}\,d\theta \tag{D3}$$

$$F(\phi,k) = \int_0^{\phi}\frac{d\theta}{\sqrt{1-k^2\sin^2\theta}} \tag{D4}$$

Similarly, the solution for the electric potential in the electrolyte in Equation (15) can be rewritten as

$$\frac{z-z_G}{L_D} = \pm f\frac{2i}{\sqrt{2-b}}\left\{-F\left[i\frac{e\Delta\varphi_{elec}(\beta)}{4k_BT}, \frac{4}{2-b}\right] + F\left[i\frac{1}{2}\left(\frac{e\left[\varphi_{elec}(z)-V_G+\Delta V_G\right]}{k_BT} + \frac{e\Delta\varphi_{elec}(\beta)}{2k_BT} \mp \frac{c_{sem}}{c_G}\sqrt{\beta(\alpha-1)}, \frac{4}{2-b}\right)\right]\right\} \tag{D5}$$

The use of elliptic integrals enables a more accurate and fast calculation of the expressions.

Appendix E: Values of β and f for Figure 3

Figure E1a,b shows the values of the parameters β and f obtained from the numerical solution of the 2 × 2 system of equations in Equations (22) and (23) corresponding to the calculations shown in Figure 3 for, respectively, $p_S = 3{\cdot}10^{17}\,\mathrm{cm}^{-3}$ and $p_S = 6{\cdot}10^{15}\,\mathrm{cm}^{-3}$ (continuous lines). We used different colors to represent the different ranges of signs corresponding to Table 1. For comparison we also plotted the β_H values obtained in the case of an OMIS capacitor (or and OMES capacitor in the Helmholtz approximation) (grey dashed lines).

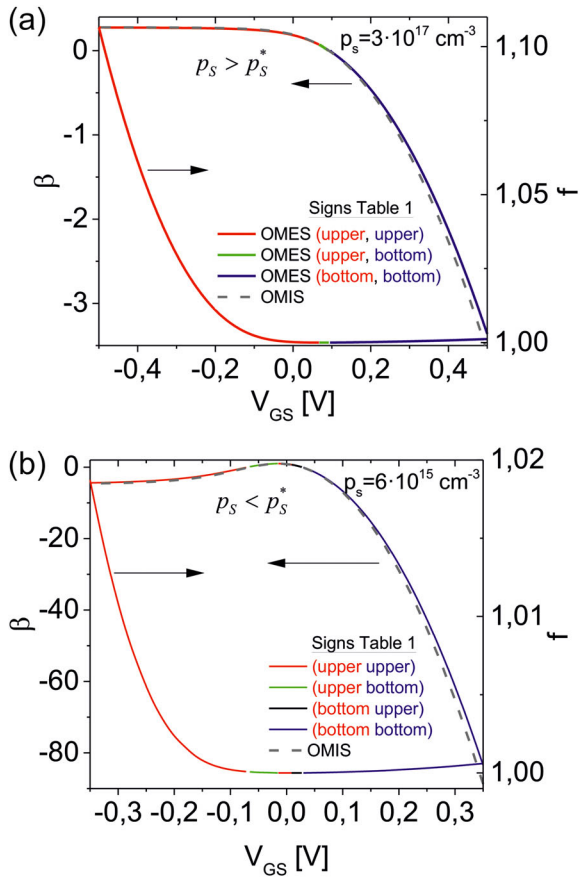

Figure E1. Values of the parameters β (left axes) and f (right axes) as a function of V_{GS}, corresponding to the calculations shown in a) Figure 3a–c and b) Figure 3d–f. The gray dashed lines represent the values of β_H in the Helmholtz approximation. Different colors correspond to the signs in Table 1.

Acknowledgements

L.H. and G.G. contributed equally to this work. The authors acknowledge useful discussions with Shubham Tanwar and the members of the BORGES Marie Skłodowska-Curie ITN network. This work has received funding from the European Union's Horizon 2020 research and innovation program under the Marie Skłodowska-Curie grant agreement No 81386 (BORGES), and from CERCA from the Generalitat de Catalunya.

Conflict of Interest

The authors declare no conflict of interest.

Data Availability Statement

The data that support the findings of this study are openly available in doi: 10.5281/zenodo.7108760.

Keywords

analytical model, metal electrolyte semiconductor capacitors, metal insulator semiconductor capacitors, organic devices

Received: September 26, 2022
Revised: October 25, 2022
Published online: November 11, 2022

[1] P. K. Manda, L. Karunakaran, S. Thirumala, A. Chakravorty, S. Dutta, *IEEE Trans. Electron Devices* **2019**, *66*, 3967.
[2] F. Torricelli, D. Z. Adrahtas, Z. Bao, M. Berggren, F. Biscarini, A. Bonfiglio, C. A. Bortolotti, C. D. Frisbie, E. Macchia, G. G. Malliaras, I. McCulloch, M. Moser, T. Q. Nguyen, R. M. Owens, A. Salleo, A. Spanu, L. Torsi, *Nat. Rev. Methods Primers* **2021**, *1*, 66.
[3] A. Groß, in *Surface and Interface Science: Volume 8: Interfacial Electrochemistry* (Ed: K. Wandelt), Wiley-VCH, Weiheim, Germany **2020**, pp. 471–515.
[4] H. Helmholtz, *Ann. Phys.* **1853**, *89*, 211.
[5] M. Gouy, *J. Phys. Theor. Appl.* **1910**, *9*, 457.
[6] D. L. A. Chapman, *Philos. Mag.* **1913**, *25*, 475.
[7] O. Stern, *Electrochemistry* **1924**, *30*, 508.
[8] D. Wang, V. Noël, P. Benoît, *Electronics* **2016**, *5*, 9.
[9] A. Kyndiah, M. Checa, F. Leonardi, R. Millan-Solsona, M. Di Muzio, S. Tanwar, L. Fumagalli, M. Mas-Torrent, G. Gomila, *Adv. Funct. Mater.* **2021**, *31*, 2008032.
[10] S. M. Sze, K. K. Ng, *Physics of Semiconductor Devices*, 3rd ed., John Wiley & Sons, Hoboken **2006**.
[11] S. Jung, C.-H. B. Y. Kim, G. Horowitz, *J. Phys. D: Appl. Phys.* **2015**, *48*, 395.
[12] G. Gomila, J. M. Rubí, *J. Appl. Phys.* **1997**, *81*, 2674.
[13] M. S. Kilic, M. Z. Bazant, A. Ajdari, *Phys. Rev. E* **2017**, *75*, 021.
[14] M. S. Kilic, M. Z. Bazant, A. Ajdari, *Phys. Rev. E* **2007**, *75*, 021.
[15] G. Palazzo, D. De Tullio, M. Magliulo, A. Mallardi, F. Intranuovo, Y. M. Mulla, P. Favia, I. Vikholm-Lundin, L. Torsi, *Adv. Mater.* **2015**, *27*, 911.
[16] N. Lago, A. Cester, N. Wrachien, M. Natali, S. Quiroga, S. Bonetti, A. Barbato, A. Rizzo, E. Benvenuti, V. Benfenati, M. Muccini, S. Toffanin, G. Meneghesso, *Org. Electron.* **2016**, *35*, 176.
[17] N. Lago, M. Buonomo, N. Wrachien, F. Prescimone, M. Natali, M. Muccini, S. Toffanin, A. Cester, *IEEE Trans. Electron Devices* **2018**, *65*, 4555.
[18] L. Kergoat, L. Herlogsson, D. Braga, B. Piro, M.-C. Pham, X. Crispin, M. Berggren, G. Horowitz, *Adv. Mater.* **2010**, *22*, 2565.
[19] L. Kergoat, L. Herlogsson, B. Piro, M. C. Pham, G. Horowitz, X. Crispin, M. Berggren, *Proc. Natl. Acad. Sci. U. S. A.* **2012**, *109*, 8394.
[20] Q. Zhang, F. Leonardi, S. Casalini, I. Temiño, M. Mas-Torrent, *Sci. Rep.* **2016**, *6*, 39.
[21] D. Tu, L. Herlogsson, L. Kergoat, X. Crispin, M. Berggren, R. Forchheimer, *IEEE Trans. Electron Devices* **2011**, *58*, 3574.
[22] L. Huetter, A. Kyndiah, G. Gomila, Analytical Physical Model for Electrolyte Gated Organic Field Effect Transistors in the Helmholtz Approximation, (under review).